Bulletin of the Seismological Society of America, Vol. 102, No. 2, pp. 479–489, April 2012, doi: 10.1785/0120100219

Significant Motions between GPS Sites in the New Madrid Region: Implications for Seismic Hazard

by Arthur Frankel, Robert Smalley, and J. Paul

Abstract Position time series from Global Positioning System (GPS) stations in the New Madrid region were differenced to determine the relative motions between stations. Uncertainties in rates were estimated using a three-component noise model consisting of white, flicker, and random walk noise, following the methodology of Langbein, 2004. Significant motions of 0.37 ± 0.07 (one standard error) mm/yr were found between sites PTGV and STLE, for which the baseline crosses the inferred deep portion of the Reelfoot fault. Baselines between STLE and three other sites also show significant motion. Site MCTY (adjacent to STLE) also exhibits significant motion with respect to PTGV. These motions are consistent with a model of interseismic slip of about 4 mm/yr on the Reelfoot fault at depths between 12 and 20 km. If constant over time, this rate of slip produces sufficient slip for an M 7.3 earthquake on the shallow portion of the Reelfoot fault, using the geologically derived recurrence time of 500 years. This model assumes that the shallow portion of the fault has been previously loaded by the intraplate stress. A GPS site near Little Rock, Arkansas, shows significant southward motion of 0.3–0.4 mm/yr (±0.08 mm/yr) relative to three sites to the north, indicating strain consistent with focal mechanisms of earthquake swarms in northern Arkansas.

Introduction

A controversy has developed over the seismic hazard in the New Madrid region of the central United States, an area within the North American tectonic plate. Historical accounts of the three largest earthquakes in 1811–1812 in the New Madrid region attest to the severe effects of these earthquakes, the shaking from which was felt as far as New England. Based on intensity data, moment magnitude estimates for the largest earthquake of this sequence, the 7 February 1812 earthquake thought to be on the Reelfoot fault, range from 7.1–7.3 (Hough and Page, 2011) to 7.8 (Bakun and Hopper, 2004) and 8 (Johnston, 1996). The 1811–1812 earthquakes caused widespread liquefaction and landsliding from strong shaking, with sand blow thicknesses also indicating large magnitudes (Tuttle *et al.*, 2002). Trenching of numerous sand blows in the New Madrid region reveals at least two previous sequences of large earthquakes, similar in size to the 1811–1812 events, occurring about 1450 and 900 A.D. (Tuttle *et al.*, 2002). Trenching across the Reelfoot fault scarp also documents that large earthquakes occurred on this fault at these times (Kelson *et al.*, 1996). Sand blows as old as 2400 B.C. have been found, proving that large earthquakes and strong shaking have occurred in the area over a period of at least 4000 years (Tuttle *et al.*, 2005). Magnitude 6 earthquakes in 1843 and 1895 were located near the ends of the New Madrid seismic zone. In addition, there is a continuing high level of seismicity of magnitude 5 and lower earthquakes in the area that illuminates the Reelfoot fault, the Cottonwood Grove fault to the southwest, and the continuation of faulting to the north (e.g., Chiu *et al.*, 1992). Some researchers contend that the current seismicity represents aftershocks of the 1811–1812 sequence (Stein and Liu, 2009), although a catalog of New Madrid earthquakes of magnitude 4.0 and greater (C. S. Mueller, personal comm, 2010) shows no decline of rate since about 1920.

The controversy over New Madrid seismic hazard arises from Global Positioning System (GPS) data collected over the past 16 years or so. Newman *et al.* (1999) found no discernible motion, within the uncertainty of the measurements, between monuments measured by campaign GPS stations in the New Madrid region. They concluded that seismic hazard assessments such as the National Seismic Hazard Maps produced by the U.S. Geological Survey have overestimated the hazard in the area. Recently, Calais and Stein (2009) reported no measurable deformation between continuous GPS sites from 2000–2009. They placed upper bounds of 0.2 mm/year for the motion between sites and 1.3×10^{-9} strain per year. They stated (p. 1442) that "the observations do not require motions different from zero during this time." This has led to stories in the media to the effect that the New Madrid region has recently "turned off" and is no longer a source of significant hazard.

Needless to say, this view could have an impact on earthquake mitigation measures in the region, such as building codes, seismic retrofit, and emergency preparedness.

The National Seismic Hazard Mapping (NSHM) Project of the U.S. Geological Survey used the paleoseismic, historic, and instrumental seismicity to quantify the hazard in the New Madrid region (Frankel *et al.*, 1996; Frankel *et al.*, 2002; Petersen *et al.* 2008). The most critical input to this hazard estimate is the recurrence time of 1811–1812-type earthquakes inferred from observations of sand blows (liquefaction) of prehistoric earthquakes. The national maps give highest weight to a 500-year average recurrence time for large earthquakes, which was derived from the 1811–1812 events and the paleoliquefaction evidence of earthquakes around 1450 and 900 A.D. (Tuttle *et al.*, 2002). The resulting assessment of high hazard for New Madrid is supported by a large group of regional experts through the NSHM workshop process (Frankel *et al.*, 1996). The consensus of regional experts attending the latest NSHM workshop in May 2006 for the central and eastern United States was that the geological and seismological evidence for high hazard in New Madrid trumped the GPS results that have multiple interpretations (Petersen *et al.*, 2008).

A key issue in the interpretation of GPS data in the central United States is the deformation model appropriate for this intraplate area. Newman *et al.* (1999) invoked a model based on an infinitely long fault at a plate boundary, in which relative displacements increase away from a locked fault, reaching the value of the relative plate motion. However, Stuart (2001) pointed out that the surface deformations would be much less for the case of a creeping fault with finite length and width embedded within a tectonic plate, such that deformations at large distances from the fault approach zero. Kenner and Segal (2000) developed a model in which the New Madrid earthquakes are driven by deformation in a weak zone at depth in the crust. They found that this model produced relatively small deformation at the surface, which is consistent with the GPS observations at that time.

In this article, we document that there is measurable and significant deformation between some of the GPS stations in the region. Although the observed motions are relatively small (about 0.4 mm/yr) compared to those at some plate boundaries, they are consistent with the amount of surface deformation expected for creep of 4 mm/yr on the deeper portion of the Reelfoot fault. This amount of creep produces enough slip for earthquakes with moment magnitudes 7.3 with return times of about 500 years on the shallow portion of the Reelfoot fault.

Data

The data for this study are position time series derived from the GPS Array for Mid-America (GAMA) network, operated by the University of Memphis (Smalley *et al.*, 2005; Smalley and Ellis, 2008). Figure 1 shows a map of the stations that have been operating since at least 2000. The

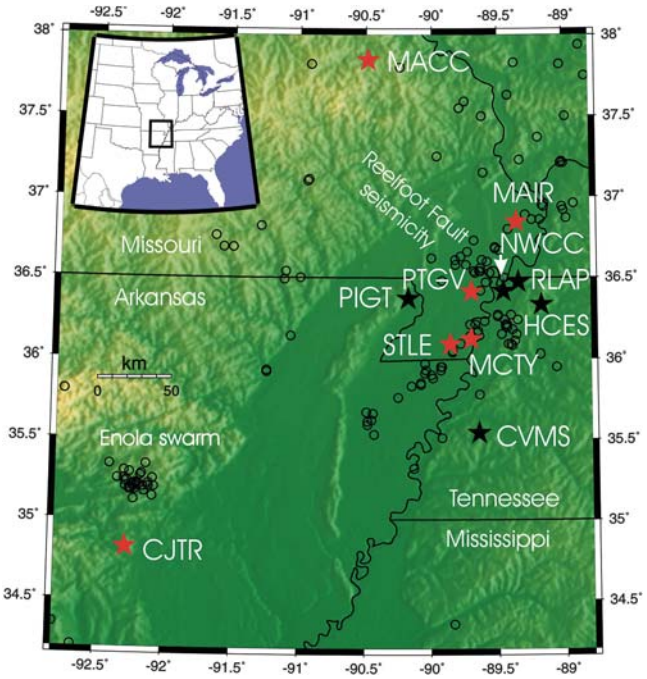

Figure 1. Map of New Madrid region showing GPS stations in the GAMA network used in this study (red stars), as well as others (black stars) that were not analyzed because of high levels of uncorrelated noise (see text). Circles are epicenters of magnitude 3.0 and larger earthquakes since 1974 from the University of Memphis, Center for Earthquake Research and Information (CERI) catalog. Rectangle in inset shows area of New Madrid region map.

processing details are given in Smalley *et al.* (2005). The position time series for these stations were derived by one of the authors of this paper (J. P.) with the GAMIT/GLOBK software package (Herring *et al.*, 2006a, b; see Data and Resources) using the three step process described in McClusky *et al.* (2000). The model of Tregoning and van Dam (2005) was applied to correct for atmospheric loading. Absolute phase center corrections were based on Schmid *et al.* (2007). The position data are referenced to ITRF2005 (Altamimi *et al.*, 2007). Stations MDO1, NLIB, GODE, CRO1, PIE1, AMC2, and AOML were utilized for stabilization for transformation to ITRF2005.

We corrected the position time series of each station for the motion of the rigid North American plate. Eric Calais (personal comm. 2010) provided his determination of the Euler pole for rigid North American plate motion based on fitting data from a set of GPS stations away from New Madrid area. This Euler pole is located at 8.3° S and 87.5° W with an angular velocity of 0.18°/Ma (Eric Calais, personal comm., 2010). For each site, we calculated the velocity from angular motion centered on this pole and adjusted the slope of the position time series so that it was with respect to stable (rigid) North America.

Figure 2 shows the horizontal position time series for all of the GAMA sites that have been operating since at least 2000, relative to rigid North American plate. The error bars plotted in Figure 2 are the standard errors from the GLOBK

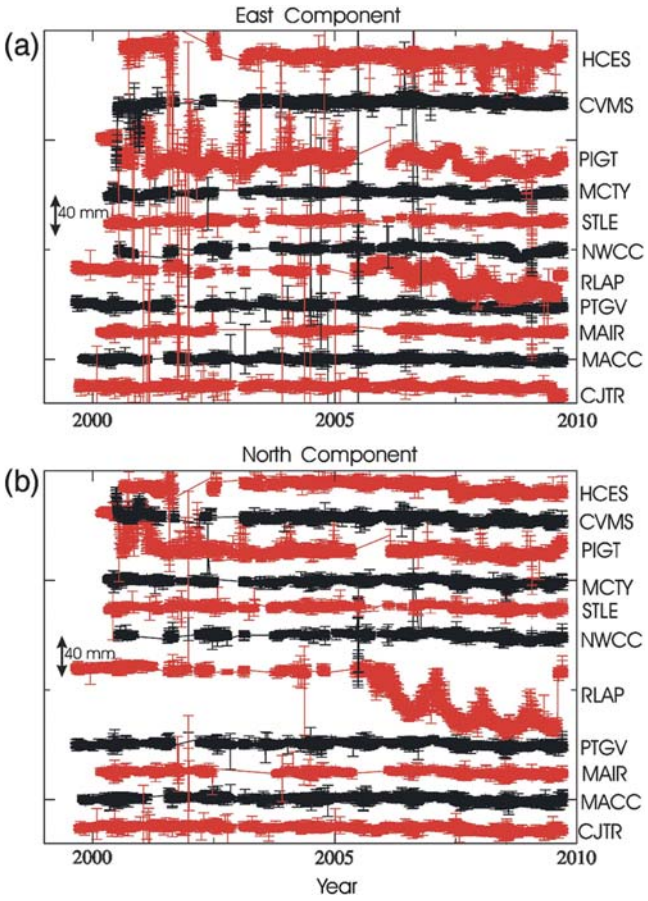

Figure 2. (a) East–west and (b) north–south position time series for stations in GAMA network that have been operating since 2000. The time series were adjusted so that they are relative to stable North America. Error bars are from the GLOBK output. Red and black colors are used so that the time series for different stations can be distinguished.

software. All position time series plotted in this paper are relative to rigid North America.

It is clear that some of the time series in Figure 2 show more long-period noise than others. We decided to only work with the position time series that showed good correlation. To quantify this, we first differenced the time series with respect to station PTGV (east–west component). Then the differential time series were fit to a line using simple linear regression. Only stations with a root mean square (rms) residual of less than 3.0 mm over the 10-yr period of the data were used in the analysis in this paper. This excluded the stations with larger amounts of uncorrelated noise. The excluded stations had rms residuals ranging from 4.5 (CVMS) to 9.9 (NWCC). Similar results were found when using STLE as the reference site. The stations we use in this paper (PTGV, STLE, MACC, MCTY, MAIR, and CJTR) have time series that show similar trends, as will be documented below (see Observations and Methodology). These stations are shown by the red stars in Figure 1.

Obviously, obtaining stable monuments in the sediments of the Mississippi embayment is difficult. The stations used in this study employ a variety of monumentation methods. Stations CJTR and MACC have pipes cemented directly into rock. The other stations in this study have *H* beams that are pile-driven into the ground. These *H* beams are 60 feet long with 10 inch flanges.

Observations and Methodology

The position time series show distinct motion between some of the sites. Figure 3 displays the position time series for stations PTGV and STLE, along with the daily error bars from the GLOBK processing. In each plot we have adjusted the position of one of the time series so that the positions of the two stations are lined up vertically in the plot at the early times. It is clear that much of the noise with periods of about a year and longer is correlated between the stations. For the east component (Fig. 3, top), there is an indication that the time series diverge with time.

This difference in the time series between STLE and PTGV is clearer on plots of the position time series without the error bars (Fig. 4). The east–west time series of STLE and

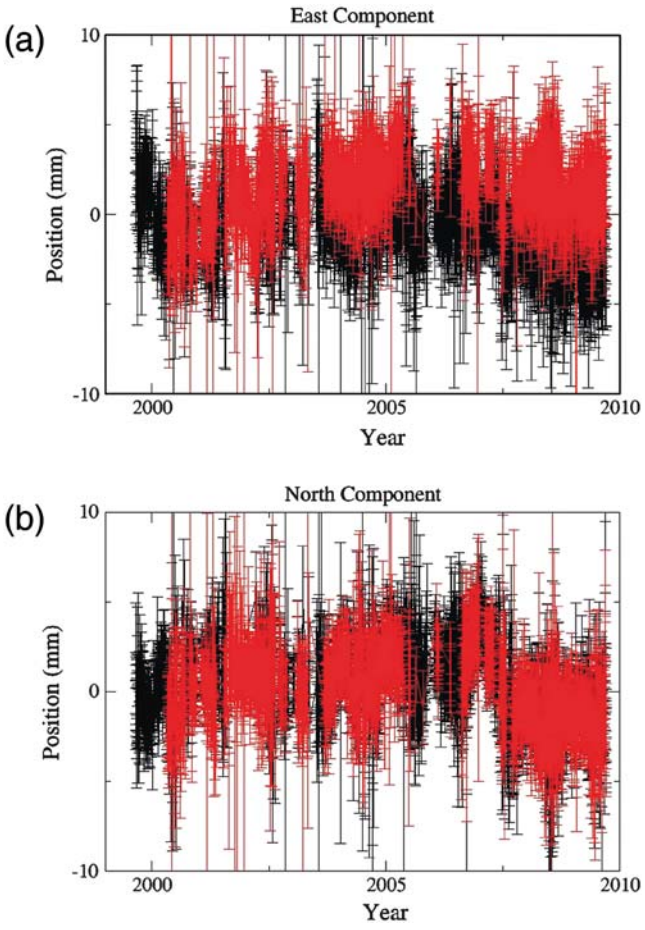

Figure 3. Position time series for PTGV (black) and STLE (red). Time series are corrected for the velocity of stable North America and aligned vertically on the plot. Error bars are from the GLOBK output.

PTGV clearly diverge with time, indicating relative motion between the two sites from 2000 to 2009. The question is whether this motion is statistically significant. The north–south component does not show apparent motion between the two sites.

We differenced the positions between the two sites at each time step to determine the relative motion and to remove the correlated noise between the stations. Some of the stations were not sampled on the same dates. We only subtracted positions between stations when the measurements were made on the same day. Figure 5 exhibits the differential time series. There is a clear downward slope to the east–west differential time series (Fig. 5, top), implying westward motion of PTGV relative to STLE. Next we describe how we estimate the rate of this motion and its uncertainty.

One of the major issues in analysis of GPS data to determine rates of motions is the estimation of the uncertainties in these rates. This estimation of uncertainties depends on the model of noise that is applied and is a topic of ongoing research.

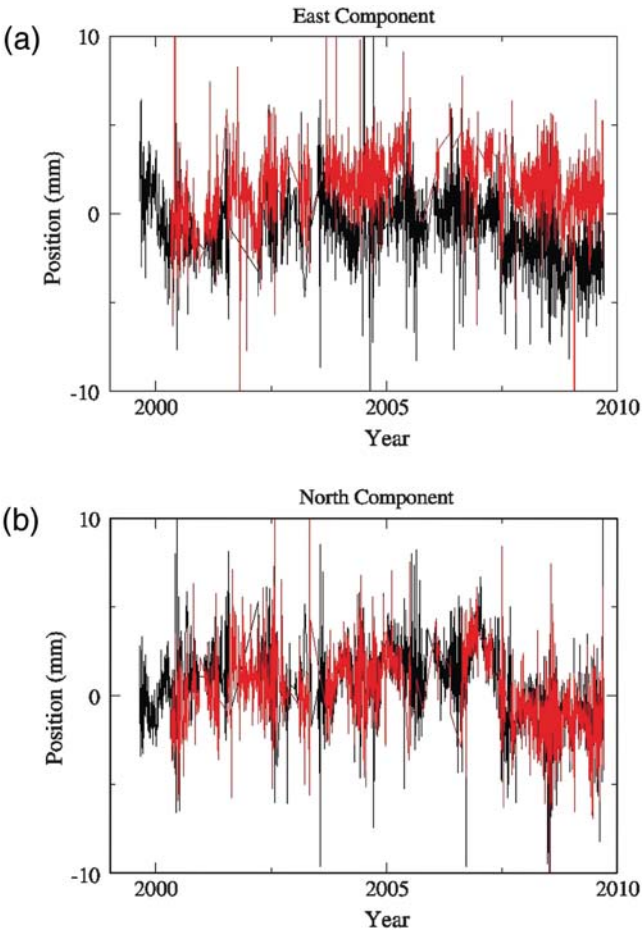

Figure 4. Position time series for PTGV (black) and STLE (red), relative to stable North America. Note the divergence of STLE and PTGV on the east–west component over time, indicating differential motion.

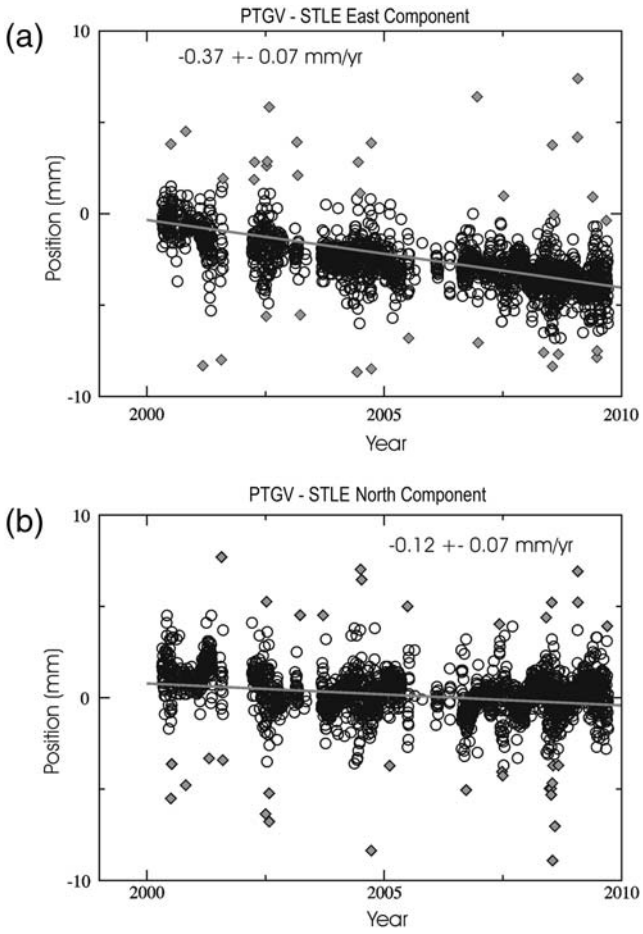

Figure 5. Differential time series of PTGV with respect to STLE, along with best-fitting rates. Uncertainties are one standard error using the white, flicker, random walk noise model. Gray lines are the best fits to the data. Note the significant downward slope of the line fitting the data for the east–west component, indicating westward motion of PTGV relative to STLE. Gray diamonds indicate outliers not used in the rate determination (see text).

In this study, rates of motion and their standard deviations were determined using a noise model consisting of three types of noise: white, flicker, and random walk (Langbein, 2004, 2008). These noise types differ in their spectral fall-off. The power spectrum of white noise is flat with frequency f. The power spectrum of flicker noise is proportional to $1/f$ and that of random walk noise is proportional to $1/f^2$.

Following Langbein (2004), the basic formula we use to describe the difference between two position time series, $d_i - r_i$, is

$$d_i - r_i = b + \nu t_i + \varepsilon_{wi} + \varepsilon_{fi} + \varepsilon_{ri} + \sum_{m=1}^{2}[a_m \sin(2\pi f_m t_i) + b_m \cos(2\pi f_m t_i)].$$

Here i is the sample number, v is the velocity between the two sites, and t_i is the time. The terms for white, flicker, and random walk noise are ε_{wi}, ε_{fi}, ε_{ri}, respectively. The summa-

tion term contains the annual and semiannual components in the time series; f_1 is one cycle per year and f_2 is two cycles per year. We used the est_noise6ac program written by John Langbein (Langbein, 2004), which estimates the rate of motion v and the offset b, along with their uncertainties based on the noise model. This program calculates maximum likelihood estimates for the spectral amplitudes of white, flicker, and random walk noise components from each differential time series. The program also determines the best fit for a_m and b_m that describe the annual and semiannual terms.

Before applying the est_noise6ac program, we removed outliers from the differential time series using the bust_4 program written by John Langbein (see Data and Resources). This program finds the running median over 180-day windows and then removes data points that are separated from the running median by greater than four times the interquartile ratio. Figure 5 shows the outliers that were removed (diamonds). All of the following plots in this paper have the outliers removed.

Based on the results using the three-component noise model (white, flicker, and random walk) the east–west velocity between STLE and PTGV in Figure 5 (top) is significant. The best-fitting line to the data (with outliers removed), given the noise model, has a rate of -0.37 ± 0.07 mm/yr. The plus and minus bounds quoted in this paper represent one standard error in the slope (rate) determination, as derived by est_noise6ac from the three-component noise model. Thus, this rate is significant to more than two standard errors (greater than 95% confidence). There is no clear slope seen in the differential time series for the north–south component (Fig. 5, bottom), and the rate is less than two standard errors.

Station CJTR near Little Rock, Arkansas, also exhibits significant motion with respect to station STLE. Figure 6 contains the time series for these two stations. For the east–west and north–south components, the time series between the stations diverge over time. Note that there is an offset in the time series for CJTR on both components toward the middle of 2009. Otherwise, the noise is well correlated between the two stations. Because of the offset, we exclude the data after June 2009 in the analysis for CJTR.

Differencing the time series reveals a trend of motion between CJTR and STLE (Fig. 7). For the north–south component, we determined a best-fitting rate of -0.43 ± 0.08 mm/yr, with CJTR moving south with respect to STLE. Again, this rate is greater than two standard errors and exceeds the 95% confidence bound. The motion for the east–west component is -0.29 ± 0.06 mm/yr. However, this motion to the west may be less compelling because it appears that the data from 2007 to 2009 do not show the same slope as the earlier data (Fig. 7).

Figure 8 displays the time series for stations MACC, MAIR, and MCTY differenced with the values at STLE, along with lines with the rates from est_noise6ac. There is statistically significant motion on the east–west components of MACC (-0.37 ± 0.12 mm/yr) and MAIR (-0.23 ± 0.03 mm/yr) relative to STLE. In these cases, the lines fit

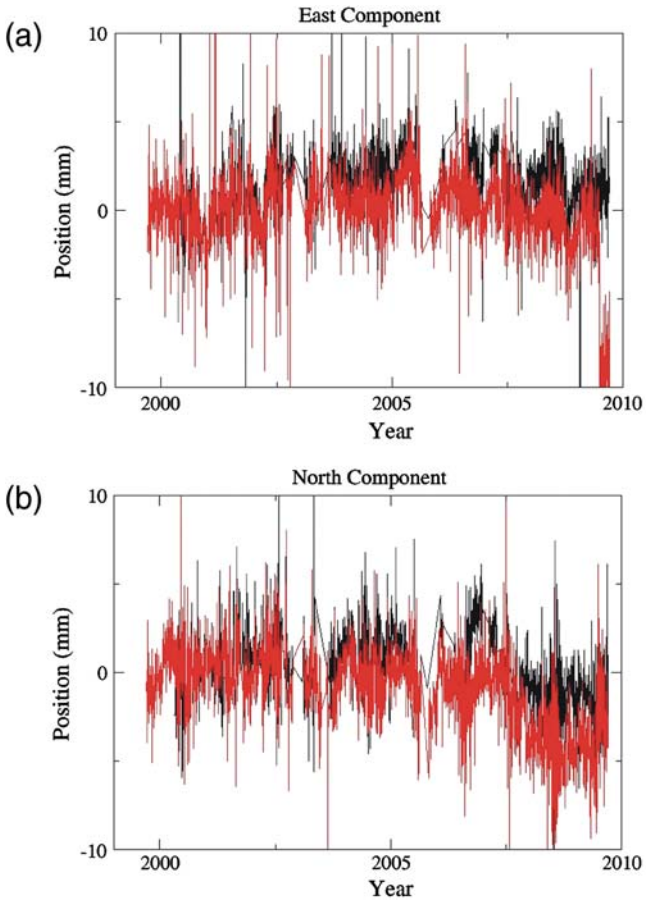

Figure 6. Position time series for CJTR (red) and STLE (black). Time series are corrected for the velocity of stable North America. Note divergence over time of time series between these stations on both components, indicating relative motion.

the trend of the data fairly well over the whole time period. While the determination of the east–west rate for MCTY–STLE shows substantial uncertainty (0.06 ± 0.38 mm/yr), the data points show no trend over the 10-yr period, indicating there is no significant motion between these sites, which are within 15 km of each other.

The north–south rates for these baselines are less than two standard errors (Fig. 8). For station MCTY, there appears to be motion of the station over the first year and then a leveling off, possibly indicating initial settling of the station.

The observed velocity vectors relative to station STLE and their uncertainties are plotted on the map in Figure 9. Table 1 lists the velocities and their standard errors. The ellipses in Figure 9 denote two standard errors (95% confidence bounds). Stations PTGV, MAIR, MACC, and CJTR show significant westward motion relative to STLE. In other words, station STLE shows significant eastward motion relative to these stations. The baselines of PTGV–STLE, MACC–STLE, and CJTR–STLE show vector magnitudes of 0.39, 0.39, and 0.52 mm/yr, respectively (Table 1).

The observed motions and strains are larger than the upper limits reported by Calais and Stein (2009) from their analyses of GPS data. The motions of 0.4 mm/yr that we

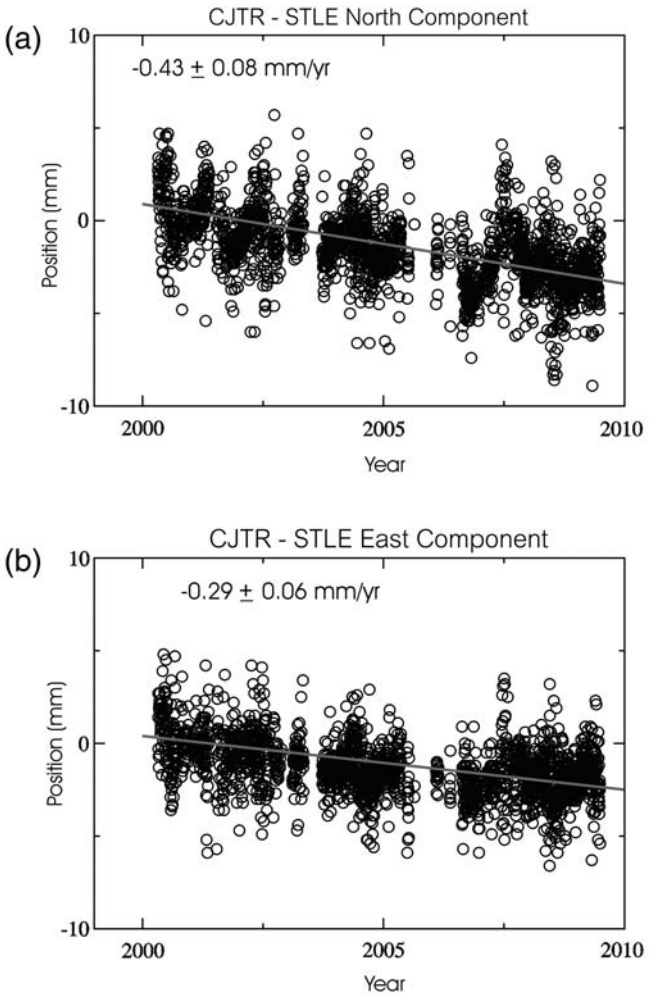

Figure 7. Differential position time series and best-fit lines (gray) for CJTR with respect to STLE. Uncertainties are one standard error using the white–flicker–random walk noise model.

found between some stations in the New Madrid seismic region are substantially higher than the 0.2 mm/yr upper limit stated in their paper. Note that station CJTR was not used in their analysis. The motion of PTGV relative to STLE over a distance of about 30 km is equivalent to a shear strain rate of 6×10^{-9} per year, about five times higher than the maximum strain rate that Calais and Stein (2009) reported was allowed by the GPS data.

Differential position time series were also calculated with respect to station PTGV (Fig. 10). The rate calculated for the east–west component of the MCTY–PTGV baseline is slightly greater than two standard errors: 0.40± 0.19 mm/yr. Thus there is significant eastward motion of MCTY relative to PTGV. This implies that the eastward motion of STLE with respect to PTGV is not an artifact of a monumentation problem at STLE. CJTR shows significant southward motion (0.32 ± 0.08 mm/yr) relative to PTGV. MACC and MAIR show motions less than 0.2 mm/yr, although they are just above two standard errors.

Figure 11 is a map with the observed rates with respect to PTGV and their 95% confidence bounds (see Table 1). Again, the eastward motion of STLE relative to PTGV is 0.37± 0.7 mm/yr. Note the large uncertainty in the north–south component of MCTY–PTGV, although the observed eastward motion is slightly above the two standard error level.

Station CJTR shows significant southward motion with respect to both PTGV and STLE. In addition, our rate calculation of CJTR with respect to MACC finds 0.26± 0.09 mm/yr of southward motion and no significant east–west motion. This southward motion of CJTR relative to stations to the north may indicate localized north–south extension near CJTR. This southward motion is generally consistent with the direction of the tension (T) axis of focal mechanisms from the nearby Enola, Arkansas, earthquake

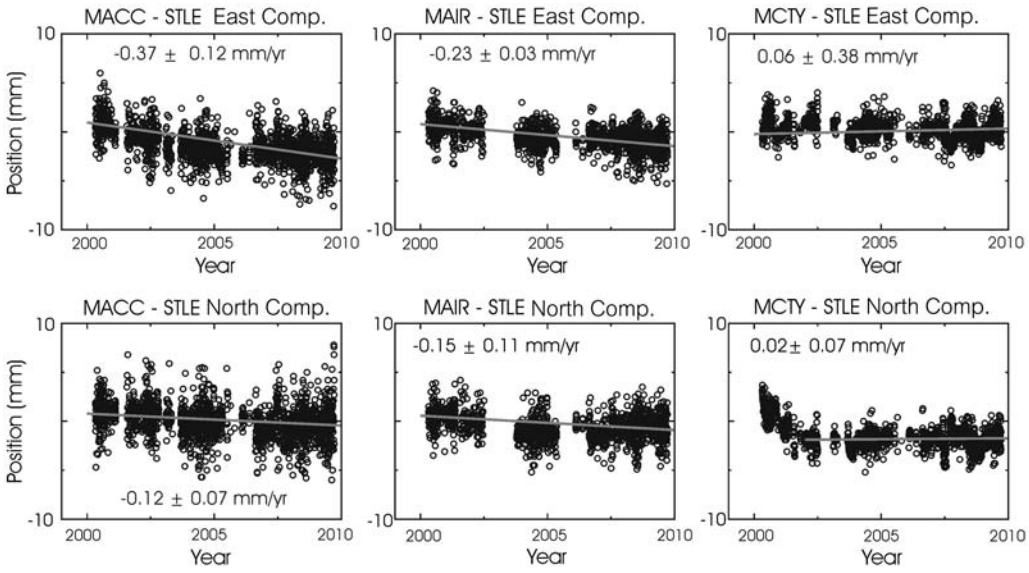

Figure 8. Differential position time series and best-fit lines (gray) for other stations, with respect to STLE. Uncertainties are one standard error.

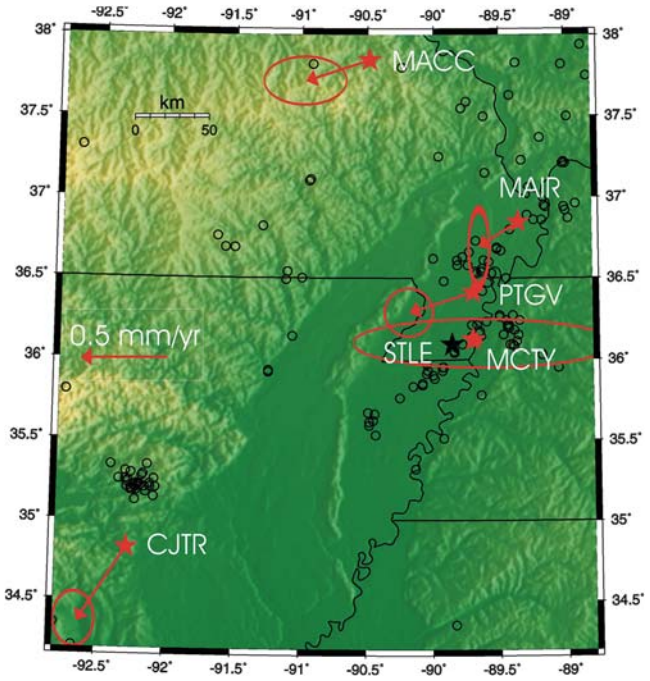

Figure 9. Map showing observed differential motions (arrows) with respect to STLE. Ellipses are the 95% confidence bounds (two standard errors).

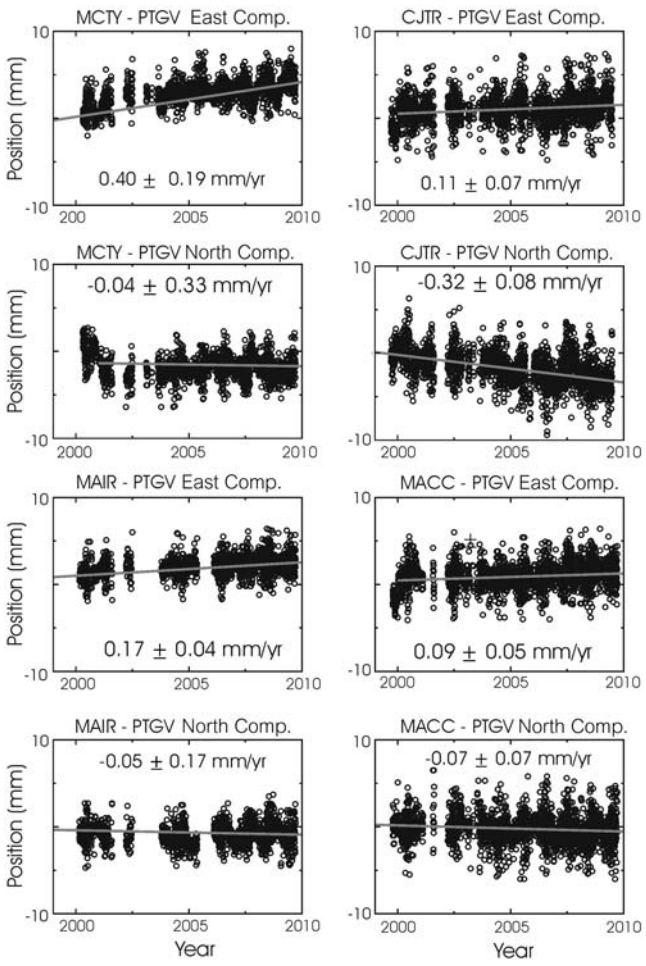

Figure 10. Differential position time series with respect to PTGV, along with best-fit lines (gray) and uncertainties (one standard error).

swarm in the 1980s and 2001 (see Fig. 1) and more recent adjacent swarm near Guy, Arkansas. Focal mechanisms for the Enola sequence typically exhibited strike-slip faulting with south to southeast striking *T* axes (Haar *et al.*, 1984; Saikia and Herrmann, 1986; Rabak *et al.*, 2010). Focal mechanisms for the more recent (2010–2011) Guy, Arkansas, swarm, which may have been induced and is located just to the west of the Enola swarm, also exhibit strike-slip faulting with southeast striking *T* axes (R. B. Herrmann, personal comm., 2011; see Data and Resources).

Model of Deep Slip on the Reelfoot Fault

We propose a model with slip at depths of 12–20 km on the Reelfoot fault as a possible explanation for the limited GPS data. We are advancing this speculative and incomplete model to demonstrate that there can be substantial interseismic slip at depth and still have the model be consistent with low rates of deformation at the surface. Here, with the added geodetic constraint, we are basically finding the same conclusions that Stuart (2001) and Kenner and Segal (2000) derived from their models. The deep slip on the fault in the model is driven by the intraplate stress.

Figure 12a shows the surface projection of this proposed creeping portion of the Reelfoot fault, along with epicenters

Table 1
Motions of GPS Stations Determined by This Study*

Station	Latitude (°N)	Longitude (°W)	Eastward Motion Relative to STLE (mm/yr)	Northward Motion Relative to STLE (mm/yr)	Magnitude of Velocity Vector Relative to STLE (mm/yr)	Eastward Motion Relative to PTGV (mm/yr)	Northward Motion Relative to PTGV (mm/yr)	Magnitude of Velocity Vector Relative to PTGV (mm/yr)
STLE	36.089	89.858	—	—	—	0.37 ± 0.07	0.12 ± 0.07	0.39
PTGV	36.413	89.700	−0.37 ± 0.07	−0.12 ± 0.07	0.39	—	—	—
CJTR	34.822	92.273	−0.29 ± 0.06	−0.43 ± 0.08	0.52	0.11 ± 0.07	−0.32 ± 0.08	0.34
MCTY	36.119	89.702	0.06 ± 0.38	0.02 ± 0.07	0.06	0.40 ± 0.19	0.04 ± 0.33	0.40
MAIR	36.847	89.357	−0.23 ± 0.03	−0.15 ± 0.12	0.27	0.17 ± 0.04	−0.05 ± 0.17	0.17
MACC	37.845	90.485	−0.37 ± 0.12	−0.12 ± 0.07	0.39	0.09 ± 0.05	−0.07 ± 0.07	0.11

*The ± symbol represents one standard error.

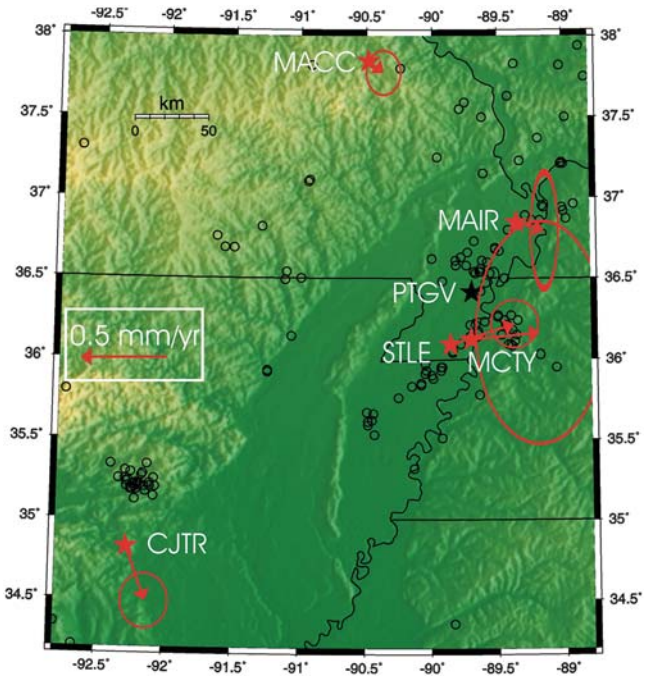

Figure 11. Map showing the observed differential motions relative to PTGV (arrows). Ellipses represent 95% confidence bounds.

determined by J. M. Chiu from the portable array for numerical data acquisition (PANDA; Chiu *et al.*, 1992). The position of the top edge of this plane was chosen to coincide with the base of seismicity. Here we are using J. M. Chiu's locations (personal comm., 2011) determined from a 1D velocity model.

The northeast–southwest cross section (Fig. 12b) indicates that the hypocenters on the Reelfoot fault dip to the southwest at 31° (Chiu *et al.*, 1992) and extend to about 12-km depth. Note that earthquakes located on the southwest arm of the New Madrid zone, the Cottonwood Grove segment (Fig. 12a), had maximum depths of about 10 km, according to Chiu *et al.* (1992).

Figure 12b illustrates that the top edge of the creeping section in our model intersects the base of seismicity at 12-km depth. We use a dip of 31° to the southwest for the creeping portion, identical to the dip of the shallow seismicity. The maximum depth of 20 km for the creeping portion was found to be a better fit to the GPS data than extending the fault to deeper depths. We specify pure thrust motion for the slip.

We calculated the surface deformations from this deep creep model using the Coulomb 3 program (see Toda *et al.*, 2005, and Lin and Stein, 2004). This program uses the Okada (1992) formulation for calculating displacements from a buried dislocation in a half-space.

We applied a weighted least-square fit to determine the slip rate on the fault (12–20-km depth) that best fits the observed differential rates. We used the rates from stations PTGV, STLE, MCTY, MACC, and MAIR. We did not use CJTR in this determination because it appears to be affected by local deformation that may not be directly related to the New Madrid zone. The data were weighted by $1/\sigma^2$, where σ is the standard error. We found a rate of 3.3 mm/yr best fit the observed rates with respect to STLE and a rate of 4.7 mm/yr best fit the observed rates relative to PTGV.

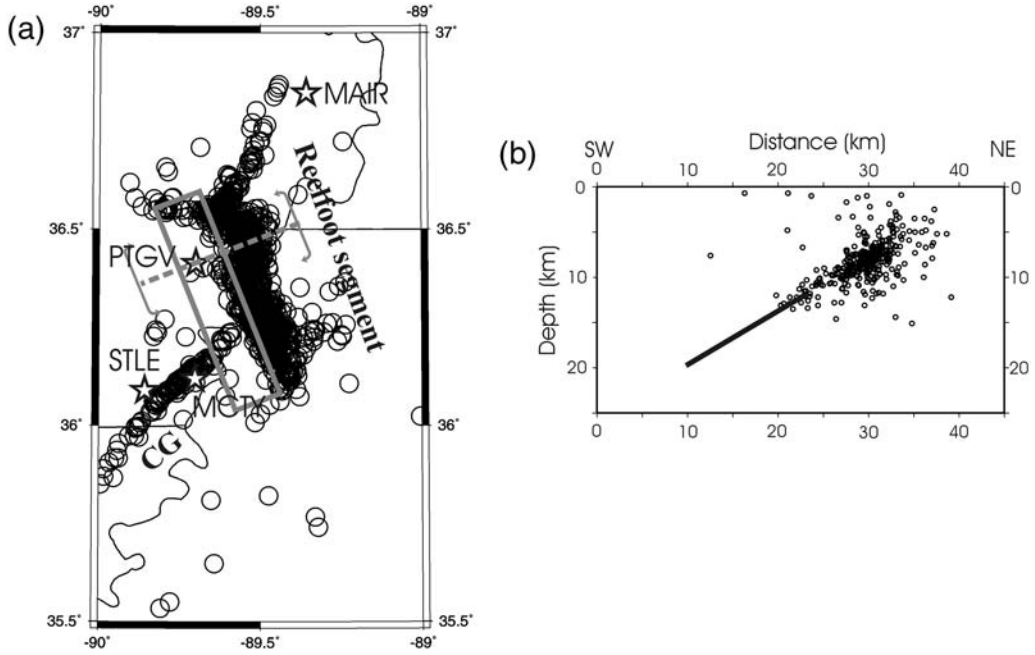

Figure 12. (a) Map with surface projection (gray rectangle) of creeping portion of the Reelfoot fault in our model and epicenters located from the PANDA array (circles; Chiu *et al.*, 1992). CG, the Cottonwood Grove segment; stars, GPS sites used in this study; dashed line, the orientation of the vertical cross section; lines at ends of dashed lines, the limits of earthquakes on either side of the dashed line that are shown in the cross section in (b). (b) Vertical cross section showing position of creeping portion of the fault in our model from 12–20 km depth (thick line) and hypocenters from Chiu *et al.* (1992). The cross section is not at the same scale as the map.

Therefore, we used 4.0 mm/yr as our preferred rate of creep in the model.

Predicted horizontal motions on the surface are only about 1/10 of the 4 mm/yr of creep at depth. Figure 13 shows the predicted surface motions relative to stable North America for 4 mm/yr of thrust motion over 12–20 km depth on the Reelfoot fault. The largest horizontal predicted motions on the surface are only about 0.5 mm/yr. The predicted horizontal motions are also fairly localized around the Reelfoot fault. Significant motions extend about 30 km eastward of the up-dip edge of the slipping portion of the fault and about 50 km westward of the down-dip edge.

The magnitudes and directions of the observed rates are consistent with this model of 4 mm/yr of deep slip on the Reelfoot fault. The model predicts little horizontal motion at station PTGV because it is located above the middle of the creeping portion of the thrust fault. Thus, the model predicts eastward motion for sites STLE and MCTY, relative to PTGV and relative to sites away from the New Madrid zone. This is what is observed in the GPS data. Figure 14 depicts the predicted and observed motions relative to PTGV. The magnitude and directions of the observed motions at STLE and MCTY are similar to the predicted values for 4 mm/yr of slip at depth. The predicted and observed motions relative to STLE are depicted in Figure 14. Now the predicted relative motions are westward. These westward motions are observed at PTGV, MAIR, and MACC, with magnitudes consistent with the model.

The mapped areas in Figures 13 and 14 do not contain stations CJTR and MACC. The model predicts virtually no deformation at these stations relative to stable North America. The model predicts 0.27 mm/yr of westward motion of MACC with respect to STLE; the observed motion is 0.37 ± 0.07 mm/yr. The predicted motion of 0.05 mm/yr of eastward motion of MACC relative to PTGV is within the one standard error uncertainty bound of the observed motions of 0.24 ± 0.20 mm/yr. The observed southern motion of CJTR may reflect localized deformation, so CJTR should not be used in the comparison with the predicted values.

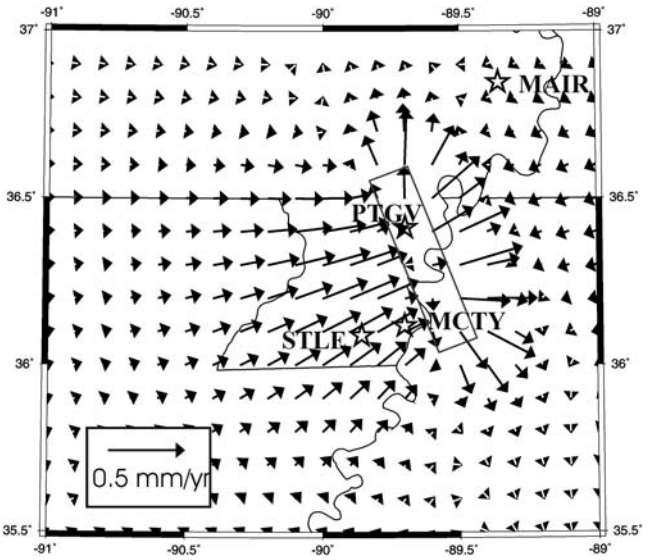

Figure 13. Predicted velocity vectors for the model with 4 mm/yr creep on the deep (12–20 km depth) portion of the Reelfoot fault. Note that the largest of predicted horizontal motions are about 1/10 of the 4 mm/yr creep at depth. The rectangle is the surface projection of the creeping portion of the fault in the model.

The model with a 4 mm/yr creep rate predicts about 1 mm/yr of uplift above the up-dip edge of the slipping portion of the fault. The noise on the vertical components of the GPS data make detection of this uplift rate problematic. Furthermore, there are no GPS stations near the location of the largest predicted uplift.

The creep rate inferred from the GPS observations can be used to estimate the magnitude of earthquakes on the shallow portion of the Reelfoot fault, given the 500-year recurrence time for 1811–1812 earthquakes found from the geological evidence. If the creep rate is constant with time, slip of 2 m will accumulate on the deep portion of the fault over 500 years. We can calculate the magnitude of the shallow portion of the fault that would produce 2 m of slip, assuming that the long-term slip between the deep and shallow portions of the fault are equal. Here we use a 60-km length and a 24-km down-dip width for the shallow seismogenic part of the fault, assuming that the rupture extends from the surface to 12-km depth. Applying a shear modulus of 3×10^{10} N/m^2, we find a seismic moment of 8.6×10^{19} N·m, which corresponds to a moment magnitude of 7.3. Thus, the GPS data are consistent with magnitude estimates for the 1811–1812 earthquakes and the geologically derived recurrence rate.

In this model, the deep slip on the Reelfoot fault triggers large earthquakes on the shallow portion of the fault. However, this model requires the shallow portion to have already been loaded by the intraplate stress. This basically follows the idea of Kenner and Segall (2000) of a zone that has been loaded sometime in the past and is gradually relaxing through a sequence of large earthquakes. We stress that the magnitude estimate of M 7.3 is consistent with the limited GPS data, assuming constant deep slip over 500 years. This analysis does not rule out the possibility that the moment magnitudes of large 1812-type earthquakes on the Reelfoot fault could be higher or lower than 7.3.

One alternative possibility is that the GPS stations are recording deformation from long-term, deep afterslip from the 1811–1812 earthquakes. An argument against this interpretation is that we would expect to also see deformation from afterslip on the Cottonwood Grove segment, which is thought to have ruptured in the December 1811 earthquake. Deep slip on this segment would produce northward motion of PTGV with respect to STLE. The data do not exhibit this northward motion, placing doubt on the afterslip hypothesis.

Conclusions

Our analysis of the limited GPS data in the New Madrid region clearly shows that there is significant motion between

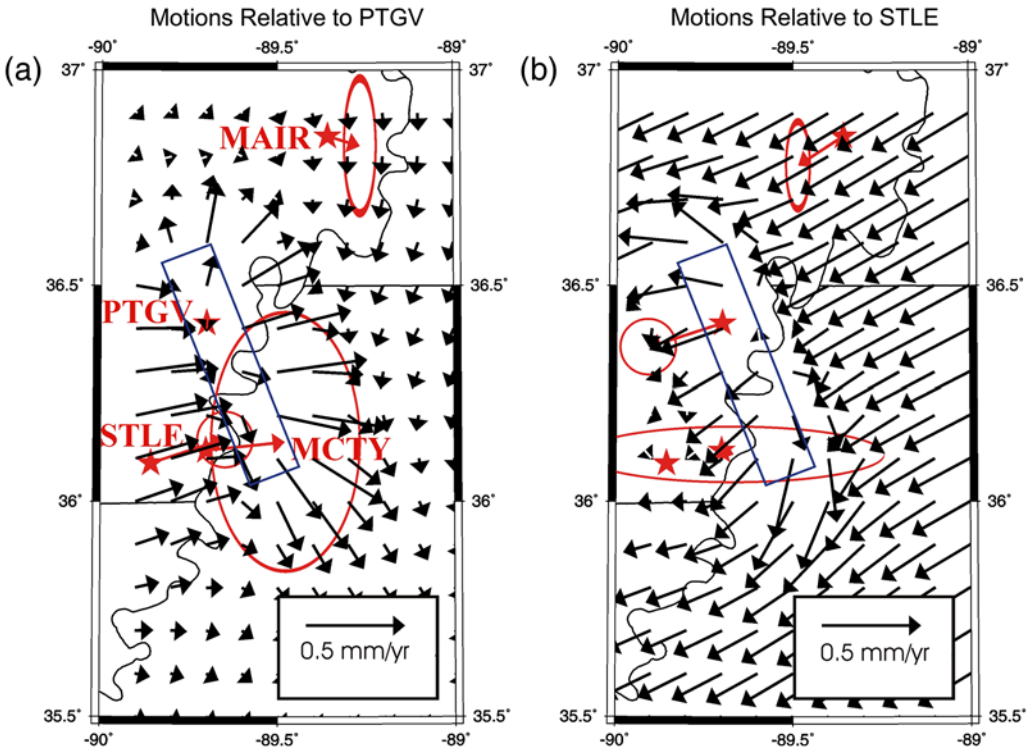

Figure 14. (a) Predicted and observed motions with respect to PTGV. Black arrows, the predicted velocities from the model with deep creep on the fault; red arrows, the observed velocities; ellipses, the 95% confidence bounds; rectangle, the surface projection of creeping portion in the model. (b) Predicted and observed motions with respect to STLE.

some of the stations. The amount of observed motion is consistent with a model of creep at depth along the Reelfoot fault. The amount of creep consistent with the GPS data could account for magnitude 7.3 earthquakes with recurrence times of 500 years. Thus, the GPS data may not conflict with the geological evidence of *M* 7–8 earthquakes with 500-year recurrence times.

There is obviously a critical need to deploy more GPS stations in the New Madrid region to better understand deformation processes in this intraplate area and to improve our assessment of seismic hazard. It is critical to install stations so as to avoid the large amounts of uncorrelated noise that is found in the time series of many of the existing stations. It is crucial to place the stations in locations where models of deep interseismic slip would predict the highest surface motions.

Data and Resources

The GPS time series is available from the University of Memphis Center for Earthquake Research and Information (CERI) web site, http://www.ceri.memphis.edu/people/gps/index.html (last accessed March 2010). The est_noise6ac program used to calculate rates and uncertainties and the program to remove outliers are available from John Langbein (ftp://ehzftp.wr.usgs.gov/langbein/est_noise/; last accessed August 2010). The seismicity catalog is from the University of Memphis (http://www.ceri.memphis.edu; last accessed December 2009). Hypocenters from the portable array for numerical data acquisition (PANDA) are available from Jer-Ming Chiu of the University of Memphis. The Coulomb program is available from http://earthquake.usgs.gov/research/modeling/coulomb/ (last accessed March 2010). Focal mechanisms of Arkansas earthquakes are available from Robert Herrmann's web site for the St. Louis University Earthquake Center (http://www.eas.slu.edu/eqc/eqc_mt/MECH.NA/; last accessed July 2011). The GAMIT-GLOBK programs are available from the Department of Earth and Atmospheric Sciences at MIT (http://www-gpsg.mit.edu/~simon/gtgk/; last accessed December 2009).

Acknowledgments

We greatly benefited from the advice and assistance of John Langbein, in helping us to better estimate the uncertainties in rates. He suggested the use of the white–flicker–random walk noise model and provided substantial guidance in applying his program for the estimation of the noise amplitudes, rate, and uncertainty. He also supplied his program to remove data outliers. We thank Oliver Boyd and Yuehua Zeng for their helpful reviews that improved the manuscript, as well as their discussions on New Madrid Global Positioning System (GPS) data. James Savage and Charles Wicks provided helpful comments that led us to make improved uncertainty estimates. We also benefited from discussions on the GPS data with Leonardo Ramirez Guzman. We thank Eric Calais for providing his pole of rotation for stable North America and for his helpful explanations of the processing of GPS data. Jer-Ming Chiu of the University of Memphis kindly provided the hypocenters he determined from the PANDA array. We thank the National Science Foundation's Mid-America Earthquake Center (NSF EEC-9701785) and

the U.S. Geological Survey Geodetic Network program for their support of the New Madrid GPS network.

References

Altamimi, Z., X. Collilieux, J. Legrand, B. Garayt, and C. Boucher (2007). ITRF2005: A new release of the International Terrestrial Reference Frame based on time series of station positions and Earth orientation parameters, *J. Geophys. Res.* **112,** no. B09401, doi 10.1029/2007JB004949.

Bakun, W. H., and M. G. Hopper (2004). Magnitudes and locations of the 1811–1812 New Madrid, Missouri, and the 1886 Charleston, South Carolina, earthquakes, *Bull. Seismol. Soc., Am.* **94,** 64–75.

Calais, E., and S. Stein (2009). Time-variable deformation in the New Madrid seismic zone, *Science* **323,** 1442, doi 10.1126/science.1168122.

Chiu, J, A. C. Johnston, and Y. T. Yang (1992). Imaging the active faults of the central New Madrid seismic zone using PANDA array data, *Seismol. Res. Lett.* **63,** no. 3, 375–394.

Frankel, A., C. Mueller, T. Barnhard, D. Perkins, E. Leyendecker, N. Dickman, S. Hanson, and M. Hopper (1996). National Seismic Hazard Maps: Documentation June 1996, *U.S. Geol. Survey Open-File Rept. 96-532*, 110 pp.; available at http://eqhazmaps.usgs.gov (last accessed December 2011).

Frankel, A., M. Petersen, C. Mueller, K. Haller, R. Wheeler, E. Leyendecker, R. Wesson, S. Harmsen, C. Cramer, D. Perkins, and K. Rukstales (2002). Documentation for the 2002 update of the National Seismic Hazard Maps, *U.S. Geol. Surv. Open-File Rept. 02-420*, 39 pp.; available at http://eqhazmaps.usgs.gov (last accessed December 2011).

Haar, L. C., J. B. Fletcher, and C. S. Mueller (1984). The 1982 Enola, Arkansas, swarm and scaling of ground motions in the eastern United States, *Bull. Seismol. Soc. Am.* **74,** 2463–2482.

Herring, T. A., R. W. King, and S. C. McClusky (2006a). GPS Analysis at MIT: GAMIT Reference Manual, Release 10.3, Department of Earth, Atmospheric, and Planetary Sciences, Massachusetts Institute of Technology, Cambridge, Massachusetts.

Herring, T. A., R. W. King, and S. C. McClusky (2006b). Global Kalmanfilter VLBI and GPS analysis program: GLOBK Reference Manual, Release 10.3, Department of Earth, Atmospheric, and Planetary Sciences, Massachusetts Institute of Technology, Cambridge, Massachusetts.

Hough, S. E., and M. Page (2011). Towards a consistent model for strain accrual and release for the New Madrid, central U.S., seismic zone, *J. Geophys. Res.* **116,** no. B03311, doi 10.1029/2010JB007783.

Johnston, A. C. (1996). Seismic moment assessment of stable continental earthquake—III. 1811–1812 New Madrid, 1886 Charleston, and 1755 Lisbon, *Geophys. J. Int.* **126,** 314–344.

Kelson, K. I., G. D. Simpson, R. B. Van Arsdale, J. B. Harris, C. C. Haraden, and W. R. Lettis (1996). Multiple Holocene earthquakes along the Reelfoot fault, central New Madrid seismic zone, *J. Geophys. Res.* **101,** 6151–6170.

Kenner, S. J., and P. Segall (2000). A mechanical model for intraplate earthquakes: Application to the New Madrid seismic zone, *Science* **289,** 2329–2332.

Langbein, J. (2004). Noise in two-color electronic distance meter measurements revisited, *J. Geophys. Res.* **109,** no. B04406, doi 10.1029/2003JB002819.

Langbein, J. (2008). Noise in GPS displacement measurements from southern California and southern Nevada, *J. Geophys. Res.* **113,** no. B05405, doi 10.1029/2007JB005247.

Lin, J., and R. S. Stein (2004). Stress triggering in thrust and subduction earthquakes, and stress interaction between the southern San Andreas and nearby thrust and strike-slip faults, *J. Geophys. Res.* **109,** no. B02303, doi 10.1029/2003JB002607.

McClusky, S., S. Balassanian, A. Barka, C. Demir, S. Ergintav, I. Georgiev, O. Gurkan, M. Hamburger, K. Hurst, H. Kahle *et al.* (2000). Global Positioning System constraints on plate kinematics and dynamics in the eastern Mediterranean and Caucasus, *J. Geophys. Res.* **105,** 5695–5719.

Newman, A., S. Stein, J. Weber, J. Engeln, A. Mao, and T. Dixon (1999). Slow deformation and lower seismic hazard at the New Madrid seismic zone, *Science* **284,** 619–621.

Okada, Y. (1992). Internal deformation due to shear and tensile faults in a half-space, *Bull. Seismol. Soc. Am.* **82,** 1018–1040.

Petersen, M., A. Frankel, S. Harmsen, C. Mueller, K. Haller, R. Wheeler, R. Wesson, Y. Zeng, O. Boyd, D. Perkins, N. Luco, E. Field, C. Wills, and K. Rukstales (2008). Documentation for the 2008 update of the United States National Seismic Hazard Maps, *U. S. Geol. Surv. Open-File Rept. 2008-1128*, 61 pp.

Rabak, I., C. Langston, P. Bodin, S. Horton, M. Withers, and C. Powell (2010). The Enola, Arkansas, intraplate swarm of 2001, *Seismol. Res. Letts.* **81,** no. 3, 549–559.

Saikia, C. K., and R. B. Herrmann (1986). Moment-tensor solutions for three 1982 Arkansas swarm earthquakes by waveform modeling, *Bull. Seismol. Soc. Am.* **76,** 709–723.

Schmid, R, P. Steigenberger, G. Gendt, M. Ge, and M. Rothacher (2007). Generation of a consistent absolute phase-center correction model for GPS receiver and satellite antennas. *J. Geodes.* **81,** no. 12, 781–798, doi 10.1007/s00190-007-0148-y.

Smalley, R., Jr., and M. A. Ellis (2008). Space geodesy and the New Madrid seismic zone, *Eos Trans. AGU* **89,** 28, doi 10.1029/2008EO280003.

Smalley, R., M. A. Ellis, J. Paul, and R. B. Van Arsdale (2005). Space geodetic evidence for rapid strain rates in the New Madrid seismic zone of central USA, *Nature* **453,** 1088–1090, doi 10.1038/nature03642.

Stein, S., and M. Liu (2009). Long aftershock sequences within continents and implications for earthquake hazard assessment, *Nature* **462,** 87–89, doi 10.1038/nature08502.

Stuart, W. D. (2001). GPS constraints on *M* 7–8 earthquake recurrence times for the New Madrid seismic zone, *Seismol. Res. Lett.* **72,** 745–753.

Toda, S., R. S. Stein, K. Richards-Dinger, and S. Bozkurt (2005). Forecasting the evolution of seismicity in southern California: Animations built on earthquake stress transfer, *J. Geophys. Res.*, **110,** B05S16, doi 10.1029/2004JB003415.

Tregoning, P., and T. van Dam (2005). Atmospheric pressure loading corrections applied to GPS data at the observation level, *Geophys. Res. Lett.* **32,** L22310, doi 10.1029/2005GL024104.

Tuttle, M. P., E. S. Schweig, J. D. Sims, R. H. Lafferty, L. W. Wolf, and M. L. Haynes (2002). The earthquake potential of the New Madrid seismic zone, *Bull. Seismol. Soc. Am.* **92,** 2080–2089.

Tuttle, M. P., E. S. Schweig, J. Campbell, P. M. Thomas, J. D. Sims, and R. H. Lafferty (2005).Evidence for New Madrid earthquakes in A.D. 300 and 2350 B.C., *Seismol. Res. Lett.* **76,** 489–501.

U.S. Geological Survey
University of Washington
Box 351310
Seattle, Washington 98195
afrankel@usgs.gov
(A.F.)

University of Memphis
Center for Earthquake Research and Information
3876 Central Ave.
Memphis, Tennessee 38152
rsmalley@memphis.edu
jpuchkyl@memphis.edu
(R.S., J.P.)

Manuscript received 12 August 2010